Journal of Materials Chemistry C

PAPER

View Article Online
View Journal | View Issue

Cite this: J. Mater. Chem. C, 2016, 4, 4675

$Ca_6La_4(SiO_4)_2(PO_4)_4O_2:Eu^{2+}$: a novel apatite green-emitting phosphor for near-ultraviolet excited w-LEDs

Yufei Xia,[a] Yan-gai Liu,*[a] Zhaohui Huang,[a] Minghao Fang,[a] Maxim S. Molokeev[bc] and LeFu Mei*[a]

Received 8th April 2016,
Accepted 11th April 2016

DOI: 10.1039/c6tc01418f

www.rsc.org/MaterialsC

A novel apatite phosphor $Ca_6La_4(SiO_4)_2(PO_4)_4O_2:Eu^{2+}$ was prepared by conventional high-temperature solid-state reaction. Phase purity was examined by XRD and XPS analysis. The crystal structure information, such as space group, cell parameters and atomic coordinates, were refined by the Rietveld method, revealing that Eu^{2+} occupied the sites of Ca^{2+} ions. Moreover, low-temperature experiments, including low-temperature PL spectra and low-temperature decay curve, were used to prove the existence of two luminescence centers in $Ca_6La_4(SiO_4)_2(PO_4)_4O_2:Eu^{2+}$. With the increase in doping concentration of Eu^{2+}, the emission wavelength shows a red shift from 498 nm to 510 nm, which is mainly caused by the increase in crystal-field splitting by Eu^{2+}. The optimized concentration of Eu^{2+} was confirmed to be 0.01, the R_c was calculated to be 20.09 Å and the energy transfer between Eu^{2+} was demonstrated to be by exchange interaction. Moreover, good thermal stability has been proved by a temperature-dependence experiment; it shows that the phosphor can maintain 55% of emitting intensity at 150 °C compared to that at room temperature. Finally, the $Ca_6La_4(SiO_4)_2(PO_4)_4O_2:Eu^{2+}$ phosphor was fabricated with commercial red ($CaAlSiN_3:Eu^{2+}$) and blue ($BAM:Eu^{2+}$) phosphor coating on a n-UV chip. This proves that this green phosphor has the potential to be used in a w-LED lamp.

1. Introduction

Nichia assembled a white light-emitting diode (w-LED) by means of a blue InGaN LED chip coated with yellow phosphor $Y_3Al_5O_{12}:Ce^{3+}$ ($YAG:Ce^{3+}$) in 1996.[1–3] At that time the w-LED was regarded as the next generation light source due to many advantages such as significant power reduction, higher luminous efficiency, longer lifetime and environmental friendliness.[4] Accordingly, enormous research efforts have been focused on the preparation of high quality w-LEDs.[5,6] Compared with Nichia's assembly method mentioned above, which shows high correlated color temperature (CCT ≈ 7750 K) and a low color rendering index (CRI ≈ 75),[7] packaging multicolor phosphors on a near-ultraviolet (n-UV) chips can provide relatively high quality white light because the emission spectra can be distributed over the entire visible range (400–800 nm).[8–10] This means that the study of high-performance single-color phosphor is meaningful.

Researchers have paid great attention to green-emitting phosphors, for instance the cordierite structure phosphor $K_{0.5}Mg_{1.5}Al_4Si_5O_{13}:Eu^{2+}$,[11] the garnet structure phosphors $Ca_2LaZr_2Ga_3O_{12}:Ce^{3+}$,[12] $Ca_2YZr_2Al_3O_{12}:Ce^{3+}$,[13] and the commercial green phosphor $(Ba,Sr)SiO_4:Eu^{2+}$. However, there is still room for improvement in some aspects such as wider emission region, better thermal stability and higher quantum efficiency. It is well known that the apatite compound has been utilized as a highly efficient host material for phosphor due to its adjustable crystal structure and its excellent thermal and physicochemical stability.[14–16] Recently, our group has reported a series of apatite solid solution phosphors $Ca_{2+x}La_{8-x}(SiO_4)_{6-x}(PO_4)_xO_2:Eu^{2+}$ (x = 0, 2, 4, and 6) whose emitting color can be adjusted from green to blue by changing the ratio of Ca to La. One of these compounds, $Ca_6La_4(SiO_4)_2(PO_4)_4O_2:Eu^{2+}$, show good potential as a commercial green phosphor. Therefore, we consider it worth investigating the crystal structure and luminescence properties of $Ca_6La_4(SiO_4)_2(PO_4)_4O_2:Eu^{2+}$ in more detail.

As discussed above, the novel apatite phosphors $Ca_6La_4(SiO_4)_2(PO_4)_4O_2:xEu^{2+}$ (x = 0.05–0.1) have been synthesized by high-temperature solid state reaction for the first time. The phase purity was examined by XRD and XPS and the crystal structure

[a] School of Materials Science and Technology, Beijing Key Laboratory of Materials Utilization of Nonmetallic Minerals and Solid Wastes, National Laboratory of Mineral Materials, China University of Geosciences, Beijing, 100083, China. E-mail: liuyang@cugb.edu.cn
[b] Laboratory of Crystal Physics, Kirensky Institute of Physics, SB RAS, Krasnoyarsk 660036, Russia
[c] Department of Physics, Far Eastern State Transport University, Khabarovsk 680021, Russia

information was analyzed by Rietveld refinement using XRD profiles. In addition, it is the first time that the low-temperature PL and PLE spectra and decay curves were utilized to demonstrate the inclusion of Eu^{2+} in the apatite phosphor. Moreover, the luminescence properties, such as PLE and PL spectra, lifetimes and thermal stability, are discussed in detail. Finally, the novel green phosphor $Ca_6La_4(SiO_4)_2(PO_4)_4O_2:Eu^{2+}$ was packaged on a u-UV LED chip (excitation wavelength 385 nm) with commercial red and blue phosphors, demonstrating the potential for it to be utilized in a w-LED.

2. Experiment

2.1 Sample preparation

The apatite phosphors $Ca_6La_4(SiO_4)_2(PO_4)_4O_2:xEu^{2+}$ (x = 0.005, 0.01, 0.02, 0.04, 0.06, 0.08, and 0.1) were synthesized by a conventional high-temperature solid-state method. Based on the stoichiometric amounts of reactants, Ca_2CO_3 (analytical reagent, AR), La_2O_3 (AR), SiO_2 (AR), $NH_4H_2PO_4$ (AR) and Eu_2O_3 (AR) were thoroughly ground in an agate mortar for 15 min. The mixed powders were then preheated for 1 h at 1000 °C in a corundum crucible to eliminate H_2O and CO_2. Subsequently, the mixtures were sintered at 1500 °C in a reductive atmosphere (H_2 10%, N_2 90%) for 4.5 h. After cooling to room temperature, the sintered samples were ground once again to prepare for further measurements.

2.2 Characterization

The X-ray diffraction (XRD) data of the series of phosphors were measured on an X-ray powder diffractometer (D/max-IIIA, Rigaku, Japan) with a stepwise scanning mode over the 2θ range 10°–110° using Cu-K_α radiation (1.5406 Å) with operating voltage 40 kV and current 100 mA. The XRD patterns, used in Rietveld refinement, were acquired with a step size of 0.02° and counting time of 2 s per step. X-ray photoelectron spectroscopy (XPS) measurements were collected with a Kratos Axis Ultra DLD, employing MCP stack & delay-line photoelectron detector with scanned & snapshot spectroscopy modes. The photoluminescence emission (PL) spectrum and the photoluminescence excitation (PLE) spectrum at 298 K and 8 K were measured using a Hitachi F-4600 fluorescence spectrophotometer (Japan) equipped with a 150 W Xe lamp as the excitation source. The temperature-dependent luminescence properties were measured on the same spectrophotometer, which was assembled with a computer-controlled electric furnace and a self-made heating attachment. The room-temperature luminescence decay curves were obtained from a spectrofluorometer (Horiba, Jobin Yvon TBXPS) using tunable pulsed laser irradiation (nano-LED) as the excitation. Quantum efficiency was measured by a Fluoromax-4 spectrofluorometer with an integral sphere at room temperature (Horiba, Jobin Yvon).

3. Results and discussion

3.1 Phase formation and structural characteristics

The XRD profiles of $Ca_6La_4(SiO_4)_2(PO_4)_4O_2:xEu^{2+}$ (x = 0.005–0.1) phosphors are displayed in Fig. 1. As shown in Fig. 1, all the

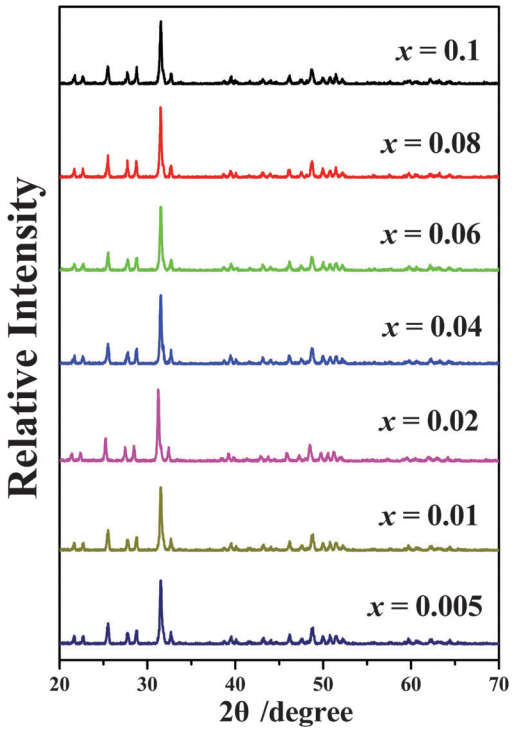

Fig. 1 The XRD traces of $Ca_6La_4(SiO_4)_2(PO_4)_4O_2:xEu^{2+}$ (x = 0.005–0.1) phosphors.

diffraction spectra do not contain any peaks from impurities or raw materials even at x = 0.1, indicating that pure apatite structure phosphors $Ca_6La_4(SiO_4)_2(PO_4)_4O_2:xEu^{2+}$ (x = 0.005–0.1) have been synthesized successfully and that doping of Eu^{2+} does not cause any impurities or phase transitions.[17] Fig. 2 depicts the photoelectron survey spectrum of the $Ca_6La_4(SiO_4)_2(PO_4)_4O_2:0.01Eu^{2+}$ sample. It contains several photoelectron peaks corresponding to O 2s, Si 2p, P 2p, La $4p_{3/2}$, Ca 2p, Ca 2s, O 1s, La $3d_{5/2}$, La $3d_{3/2}$ and Eu $3d_{5/2}$ emissions. In addition, the high-resolution XPS spectrum at the Eu $3d_{5/2}$ position is shown in the inset of Fig. 2. The binding energy was measured to be 1127 eV, which matches well with the signal of Eu^{2+} $3d_{5/2}$, demonstrating the existence of Eu^{2+}.[18]

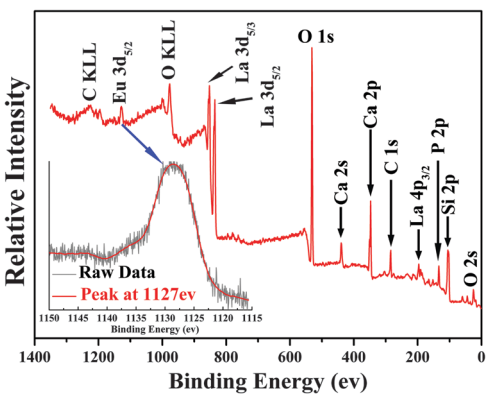

Fig. 2 Photoelectron survey spectrum of the $Ca_6La_4(SiO_4)_2(PO_4)_4O_2:0.01Eu^{2+}$ phosphor. Inset: the high resolution XPS spectrum at Eu 3d.

The crystal structure information of $Ca_6La_4(SiO_4)_2(PO_4)_4O_2$:$0.01Eu^{2+}$ was determined by the Rietveld refinement method. The observed (×), calculated (red) and difference (gray) XRD profiles for $Ca_6La_4(SiO_4)_2(PO_4)_4O_2$:$0.01Eu^{2+}$ are illustrated in Fig. 3 and the refinement parameters are presented in Table 1. The refinement results further prove that the novel apatite phosphor is a single phase without any impurity or secondary phase and that $Ca_6La_4(SiO_4)_2(PO_4)_4O_2$:$0.01Eu^{2+}$ crystallizes as a hexagonal structure with space group $P6_3/m$. The lattice parameters were determined to be $a = b = 9.536$ Å, $c = 7.026$ Å, $V = 553.35$ Å^3 and the refinement R factors finally converged to $R_{wp} = 8.17\%$, $R_{exp} = 1.28\%$, $R_p = 6.20\%$, indicating that the refined crystal structure agrees well with the starting model ($Ca_2La_8(SiO_4)_6$). In addition, all atoms positions and occupancy factors for $Ca_6La_4(SiO_4)_2(PO_4)_4O_2$:$0.01Eu^{2+}$ are listed in Table 1.

Fig. 4 illustrates the reflectance spectra of the $Ca_6La_4(SiO_4)_2(PO_4)_4O_2$ host and $Ca_6La_4(SiO_4)_2(PO_4)_4O_2$:$0.01Eu^{2+}$ in the range from 200 nm to 800 nm. Obviously, compared with the absorption characteristics of $Ca_6La_4(SiO_4)_2(PO_4)_4O_2$ host, which barely absorbs n-UV light, $Ca_6La_4(SiO_4)_2(PO_4)_4O_2$:$0.01Eu^{2+}$ shows a broad absorption band from 200 nm to 450 nm, demonstrating the as-prepared phosphor can efficiently excited by a UV or n-UV LED chip.[10,18] Furthermore, as shown in the inset of Fig. 4, the band gap of $Ca_6La_4(SiO_4)_2(PO_4)_4O_2$:$0.01Eu^{2+}$ was estimated to be 3.39 eV.

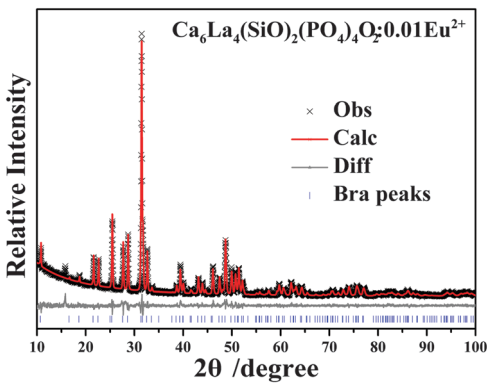

Fig. 3 Powder XRD pattern (×) of $Ca_6La_4(SiO_4)_2(PO_4)_4O_2$:$0.01Eu^{2+}$ samples with corresponding Rietveld refinement (red) and residual (gray) traces.

Table 1 Results of structure refinement of CLSPO:$0.01Eu^{2+}$

Formula					CLSPO:$0.01Eu^{2+}$
Space group					$P6_3/m$
$a = b$; c (Å)					9.536(3); 7.026(3)
V (Å^3)					553.35(5)
R_{wp} (%)					8.17
R_{exp} (%)					1.28
R_p (%)					6.20
Atom	Site	x	y	z	Occupancy
La1	6h	0.227(2)	0.983(3)	0.25	0.617
Ca1	6h	0.227(2)	0.983(3)	0.25	0.368
Eu1	6h	0.227(2)	0.983(3)	0.25	0.005
La2	4f	2/3	1/3	0.0024(1)	0.060
Ca2	4f	2/3	1/3	0.0024(1)	0.935
Eu2	4f	2/3	1/3	0.0024(1)	0.005
Si	6h	0.406(8)	0.375(1)	1/4	1/3
P	6h	0.406(8)	0.375(1)	1/4	2/3
O1	6h	0.598(2)	0.464(2)	1/4	—
O2	6h	0.339(2)	0.493(2)	1/4	—
O3	12i	0.344(1)	0.261(1)	0.072(1)	—
O4	2a	0	0	1/4	—

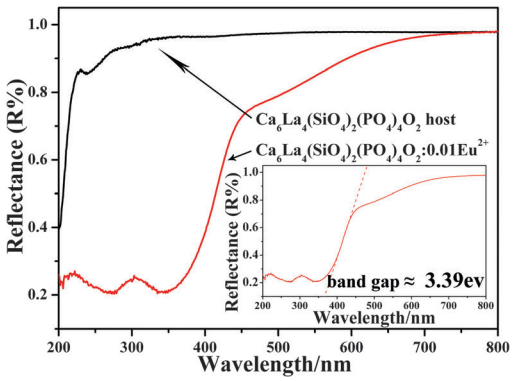

Fig. 4 Reflectance spectra of $Ca_6La_4(SiO_4)_2(PO_4)_4O_2$ host and $Ca_6La_4(SiO_4)_2(PO_4)_4O_2$:$0.01Eu^{2+}$. Inset: the band gap of $Ca_6La_4(SiO_4)_2(PO_4)_4O_2$:$0.01Eu^{2+}$.

The crystal structure of 2 × 2 × 2 unit cells, the coordination environments of a single unit cell and the coordination environments of cation sites in $Ca_6La_4(SiO_4)_2(PO_4)_4O_2$:$Eu^{2+}$ are displayed in Fig. 5a–d. As observed from Fig. 5a, $Ca_6La_4(SiO_4)_2(PO_4)_4O_2$ has a layered structure and two types of cation sites included in it, the inner-laminar site labeled M(I) with the local symmetry C_3 and the inter-laminar site labeled M(II) with the local symmetry C_s. Furthermore, Fig. 5b–d depicts the coordination environments of these cation sites. The M(I) site (located at position 4f), surrounded by 9 oxygen atoms, forms a mono-caped square antiprism and connects with the tetrahedral PO_4/SiO_4 groups. On the other hand, the M(II) site (located at position 6h) surrounded by 7 oxygen atoms forms a pentagonal bipyramid and connects with each other through vertices. Furthermore, considering the effective ionic radii (Å) of Ca^{2+} ($R_{CN=9} = 1.18$, $R_{CN=7} = 1.06$), La^{3+} ($R_{CN=9} = 1.21$, $R_{CN=7} = 1.10$) and Eu^{2+} ions ($R_{CN=9} = 1.3$, $R_{CN=7} = 1.2$), Eu^{2+} is expected to substitute the Ca^{2+} site in the $Ca_6La_4(SiO_4)_2(PO_4)_4O_2$:$Eu^{2+}$ crystal structure based on its similar ion radius and valence.[19,20]

3.2 Photoluminescence characteristics

The PLE spectrum of $Ca_6La_4(SiO_4)_2(PO_4)_4O_2$:$0.01Eu^{2+}$ (monitored at 500 nm) and the PL spectra of $Ca_6La_4(SiO_4)_2(PO_4)_4O_2$:$xEu^{2+}$ (x = 0.005–0.1) (under 365 nm excitation) are displayed in Fig. 6a and b, respectively. Due to the $4f^7 \rightarrow 4f^65d^1$ transition of Eu^{2+}, the PLE spectrum depicts a broad excitation band ranging from 280 nm to 400 nm with a maximum value at 330 nm, indicating that the $Ca_6La_4(SiO_4)_2(PO_4)_4O_2$:$Eu^{2+}$ phosphor can be suitably excited by a n-UV LED chip.[21] The PL spectrum consists of an asymmetric broad emission band peaking at 500 nm, which is ascribed to the electric dipole-allowed transition of Eu^{2+} from the lowest level of the 5d excited state to the 4f ground state.[22] In general, the asymmetric emission band is due to the different coordination environments of Eu^{2+}. As shown in Fig. 6c, the asymmetric emission band of $Ca_6La_4(SiO_4)_2(PO_4)_4O_2$:$0.01Eu^{2+}$ has been resolved

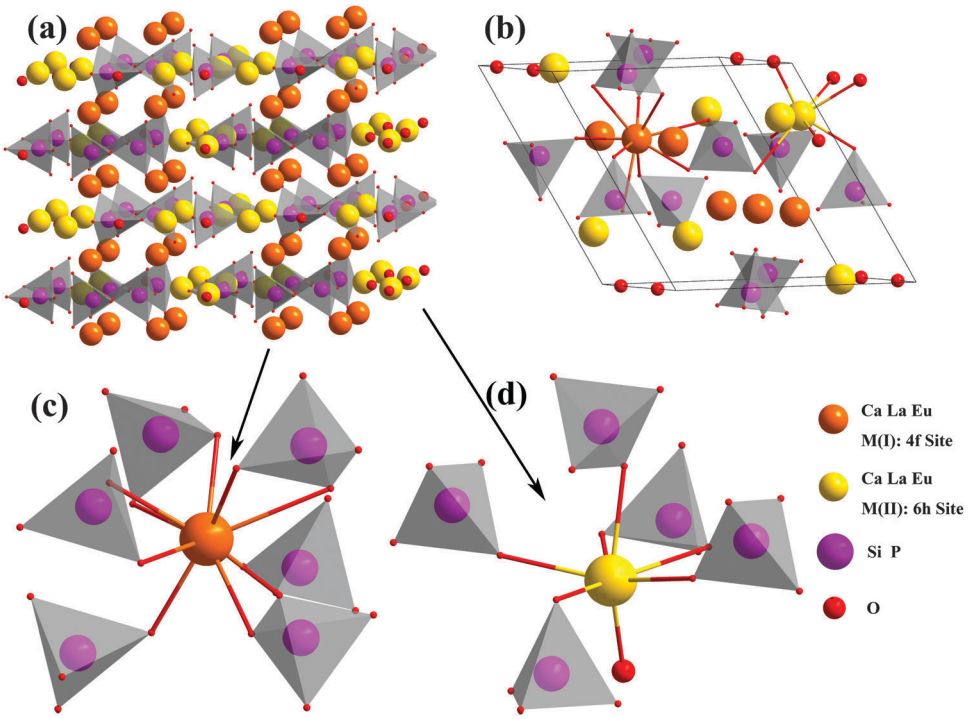

Fig. 5 (a) The crystal structure of 2 × 2 × 2 unit cells of $Ca_6La_4(SiO_4)_2(PO_4)_4:Eu^{2+}$, (b) the coordination environments in a single unit cell, (c) the coordination environment of the M(I) site with the local symmetry C_3 and (d) the M(II) site with the local symmetry C_s.

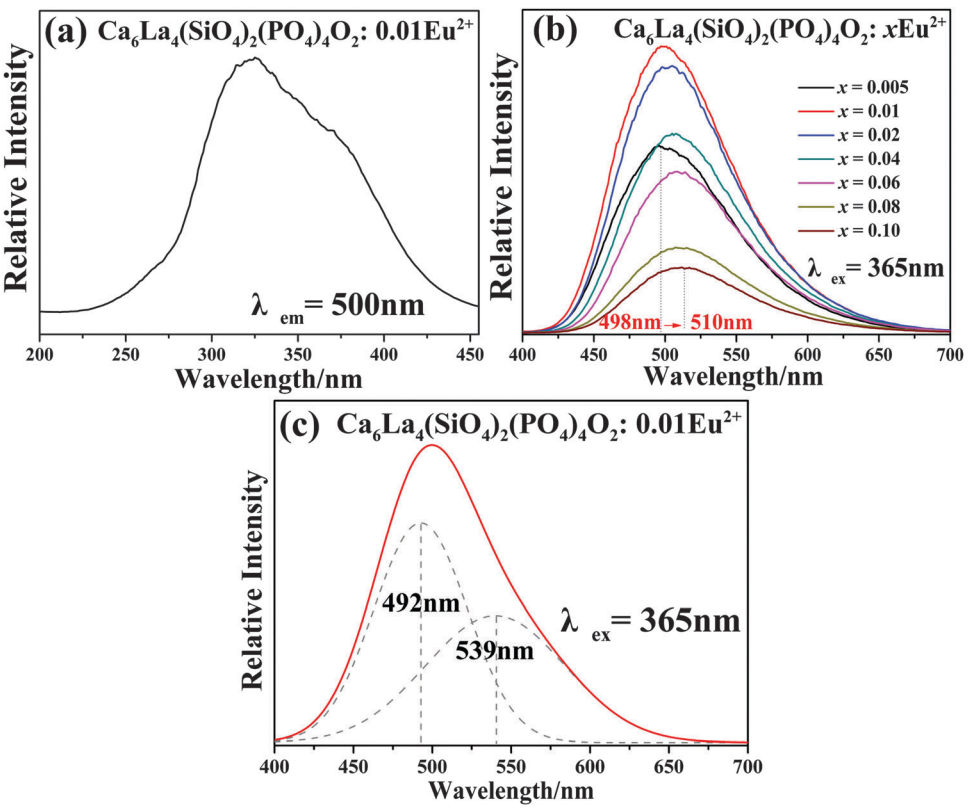

Fig. 6 (a) The PLE spectrum of $Ca_6La_4(SiO_4)_2(PO_4)_4O_2:0.01Eu^{2+}$, (b) the PL spectra of $Ca_6La_4(SiO_4)_2(PO_4)_4O_2:xEu^{2+}$ (x = 0.005–0.1) and (c) two Gaussian components of the peak of $Ca_6La_4(SiO_4)_2(PO_4)_4O_2:0.01Eu^{2+}$.

into two Gaussian components peaking at 492 nm (I1) and 593 nm (I2). Thus, the low-temperature (8 K) PLE and PL spectra of $Ca_6La_4(SiO_4)_2(PO_4)_4O_2$:0.01$Eu^{2+}$ are displayed in Fig. 7a and b to demonstrate the existence of the different Eu^{2+} sites. Consequently, the PL spectrum at low temperature contains two component peaks located at 529 nm and 584 nm and the shape of PLE spectrum was found to be identical to that of measured at room temperature. These features further prove that Eu^{2+} occupies two types of Ca^{2+} sites to form different emitting centers.[4] Moreover, due to the existence of multi-emitting centers, the $Ca_6La_4(SiO_4)_2(PO_4)_4O_2$:$Eu^{2+}$ phosphor shows a wider emission band compared with the $BaMgSiO_4$:Eu^{2+} and $Ca_2YZr_2Al_3O_{12}$:Ce^{3+} green phosphors[13,23] and it reaches a similar level as the commercial green phosphor (Ba,Sr)SiO_4:Eu^{2+}.

In theory, the width of the crystal-field splitting of the Eu^{2+} 5d level is the main influence on the position of the Eu^{2+} emitting energy level,[24] *i.e.*, the lower the lowest crystal-field position, the lower the emission energy.[25] The major difference between the 4f and 6h site is that the 6h site has a free oxygen ion, which does not belong to any silicate group. Therefore, the binding strength is not saturated compared with the 4f site resulting in the average covalency of the 6h site being higher than that of the 4f site. Consequently, Eu^{2+} will have lower emission bands when located at the 6h site than when at the 4f site and the higher energy emission band (492 nm) can be assigned to Eu^{2+} (4f) while the lower energy emission band (539 nm) is derived from Eu^{2+} (6h).[16]

This inferred conclusion can be further demonstrated by an empirical relationship proposed by Van Uitert:[15]

$$E\ (\mathrm{cm}^{-1}) = Q^{*}\left[1 - \left(\frac{V}{4}\right)^{1/V} \times 10^{-(nE_a r)/80}\right] \qquad (1)$$

where E represents the position of the d-band edge energy for rare-earth ions (cm^{-1}), Q is the position energy for the lower d-band edge for the free ion (34 000 cm^{-1} for Eu^{2+}); V is the activator ion valence (for Eu^{2+} $V = 2$), n represents the number of anions in the immediate shell about the Eu^{2+} ion, r is the host cation radius that is replaced by the Eu^{2+} ion (in Å), and E_a is the electron affinity of the atoms that form anions (in eV). In general, due to the complexity of the local crystal structure, the exact energy levels of Eu^{2+} at a specific site are hard to calculate precisely.[26] However, it can be deduced approximately that the value of E is proportional to the quantity of n and r.[4] For the as-prepared phosphors, r is equal because both of the substitutions occurring at cation sites are that Ca^{2+} is replaced by Eu^{2+}. Therefore, the band peak at 492 nm is ascribed to the $4f^6 5d^1 \rightarrow 4f^7$ transition of Eu^{2+} occupying the M(I) site with nine-coordination, whereas the longer wavelength band can be attributed to Eu^{2+} occupying the M(II) site with seven-coordination.

In addition, as shown in Fig. 6b, with the increase of doping concentration of Eu^{2+}, the peak emission wavelength shows an obvious red-shift from 498 to 510 nm. The red-shift phenomenon is mainly due to the variation in the crystal-field splitting of Eu^{2+}. In this regard, the crystal-field splitting of Eu^{2+} can be determined as obeying:[1]

$$\mathrm{Dq} = \frac{ze^2r^4}{6R^5} \qquad (2)$$

where Dq is a measure of the energy level separation, z represents the charge or valence of the anion, R is the distance from the central ion to its ligands, e is the charge of an electron, and r is the radius of the d wave function. For the $d_{(Eu-O)}$-orbital, while z, e and r are equal, then Dq is merely a function of $1/R^5$. Along with the small Ca^{2+} substituted by the larger Eu^{2+}, the distance between Eu^{2+} and O^{2-} becomes shorter and the magnitude of the crystal-field strength increases.[27] In consequence, the crystal-field splitting of the Eu^{2+} ion increases, which causes a decrease in the emission energy from the 5d excited state to the 4f ground state and a resultant red-shift.[1,13,28]

The concentration dependence of the PL intensity of the as-prepared samples $Ca_6La_4(SiO_4)_2(PO_4)_4O_2$:$xEu^{2+}$ (x = 0.005–0.1) are depicted in Fig. 8. With the increase of Eu^{2+} content, the PL intensity shows an increase at first and it reaches the maximum value at x = 0.01. Subsequently, the intensity tends to decrease gradually due to the concentration quenching effect. Thus, the optimized concentration of Eu^{2+} was confirmed to be 0.01.

In general, concentration quenching can occur in a compound by obeying two mechanisms: exchange interaction and multipolar interaction.[25,29,30] In consequence, as shown in Fig. 9, the concentration quenching originates from energy loss at a 'killer' center owing to the transfer of excitation energy among activators at a

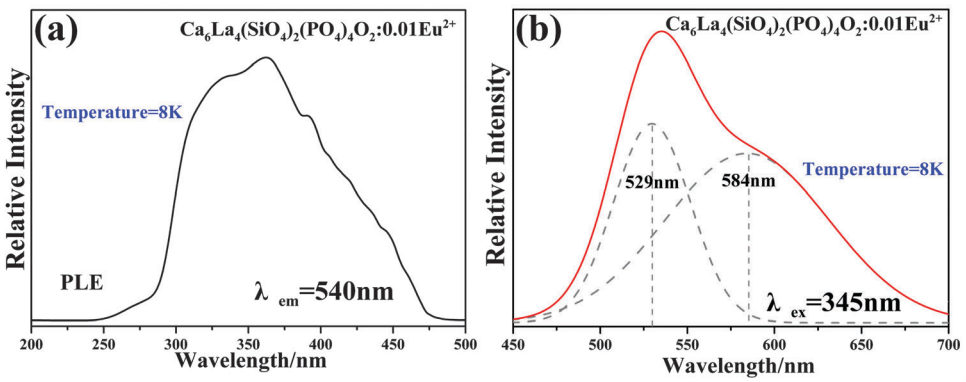

Fig. 7 (a) Low-temperature (8 K) PLE and (b) PL spectra of $Ca_6La_4(SiO_4)_2(PO_4)_4O_2$:0.01$Eu^{2+}$.

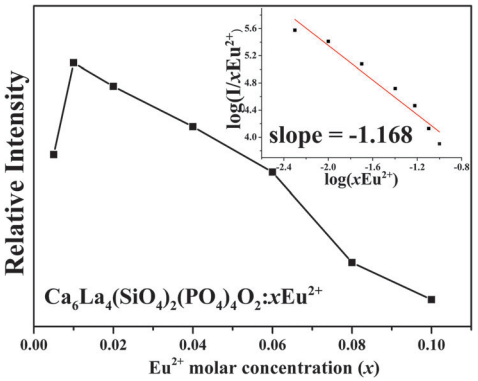

Fig. 8 The concentration dependence of the PL spectral intensity. Inset: the curve of $\log(I/x\mathrm{Eu}^{2+})$ *versus* $\log(x\mathrm{Eu}^{2+})$.

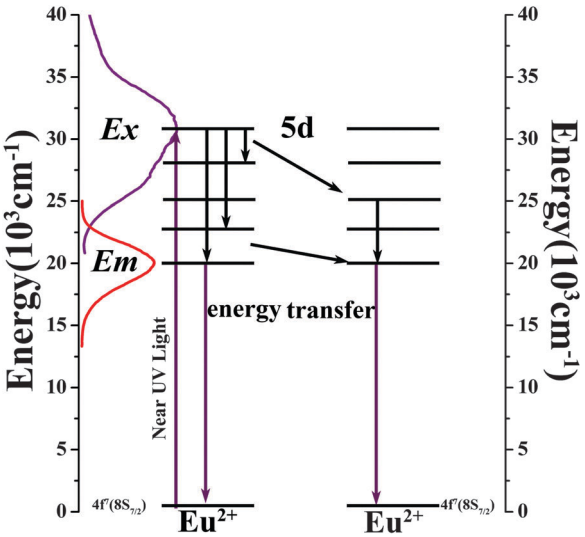

Fig. 9 Excitation energy transfer between Eu^{2+}.

relative higher concentration.[17,31] The mechanism of energy transfer between the Eu^{2+} can be expressed by the following equation:[32]

$$\frac{I}{x} = \frac{k}{1+\beta(x)^{\theta/3}} \quad (3)$$

where x is the concentration of activator, k and β are constants for each interaction for a given host lattice. Van Uitert has defined $\theta = 3$ for the exchange interaction and $\theta = 6$, 8, 10 correspond to dipole–dipole, dipole–quadrupole, quadrupole–quadrupole interactions, respectively. As depicted in the inset of Fig. 8, one can observe that the $\log(I/x\mathrm{Eu}^{2+})$ showed a relatively linear relationship with $\log(x\mathrm{Eu}^{2+})$ and that the slope was calculated to be −1.168. In consequence, the value of θ was found to be approximately 3, demonstrating the energy transfer type is exchange interaction.

Therefore, as proposed by Blasse, the critical energy transfer distance (R_c) can be calculated as follows:[4,13]

$$R_c \approx 2\left[\frac{3V}{4\pi x_c N}\right]^{1/3} \quad (4)$$

where V is the volume of the unit cell, x_c is the critical concentration of Eu^{2+} ions and N is the number of total Eu^{2+} sites in the unit cell. For $Ca_6La_4(SiO_4)_2(PO_4)_4O_2{:}x\mathrm{Eu}^{2+}$, $V = 552.5$ Å^3 and $N = 13$. Thus, the $R_{\mathrm{Eu-Eu}}$ distance was determined to be 25.32, 20.09, 15.95, 12.66, 11.06, 10.05, 9.33 and 8.78 Å when $x = 0.005$, 0.01, 0.02, 0.04, 0.06, 0.08 and 0.1, respectively. Accordingly, this indicates that with the increase in doping concentration of Eu^{2+}, $R_{\mathrm{Eu-Eu}}$ decreases and the crystal-field splitting of the Eu^{2+} 5d bands increased, leading to a continuous increase in the red-shift with the Eu^{2+} dopant concentration.[33] The critical concentration (x_c) of Eu^{2+} was determined to be 0.01 mol, therefore, the R_c value for energy transfer was calculated to be 20.09 Å.

Room temperature decay curves of the as-prepared phosphors, under excitation at 365 nm, were measured and are plotted in Fig. 10. Each decay curve can be well fitted with a second-order exponential function by the following equation:[4]

$$I(t) = A_1\exp(-t/\tau_1) + A_2\exp(-t/\tau_2) \quad (5)$$

where I presents the luminescence intensity; A_1 and A_2 are constants; t is time and τ_1 and τ_2 are the lifetimes for the exponential components. Furthermore, the average lifetime constant (τ^*) can be calculated as follows:[4]

$$\tau^* = (A_1\tau_1^{\,2} + A_2\tau_2^{\,2})/(A_1\tau_1 + A_2\tau_2) \quad (6)$$

The measured lifetimes monitored at 500 nm were calculated to be 412.9, 429.1, 383.4, 336.5, 257.5, 125.3 and 54.1 ns with Eu^{2+} contents = 0.005, 0.01, 0.02, 0.04, 0.06, 0.08 and 0.1, respectively. One can observe that with the increase of Eu^{2+} concentration, the measured lifetimes of Eu^{2+} increase to a maximum when $x = 0.01$ and then decrease rapidly. This phenomenon is a typical sign of energy transfer and concentration quenching.[22] The measured lifetime is also related to the total relaxation rate by:

$$\frac{1}{\tau} = \frac{1}{\tau_0} + A_{\mathrm{nr}} + P_t \quad (7)$$

where τ_0 is the radiative lifetime; A_{nr} presents the non-radiative rate ascribed to multi-phonon relaxation and P_t is the energy transfer rate between Eu^{2+} ions. The distance between Eu^{2+} ions decreases with the increase of Eu^{2+} concentration, resulting in the increases of energy transfer rate between Eu^{2+} and the probability of energy transfer to luminescent 'killer' sites. Consequently, the lifetimes show a gradually decreasing trend with the increase of Eu^{2+} concentration.[34] Moreover, the two decay components (τ_1 and τ_2) were detected in both the room-temperature and low-temperature decay curves, further demonstrating that Eu^{2+} occupies two different Ca^{2+} sites in $Ca_6La_4(SiO_4)_2(PO_4)_4O_2$ host.

In general, temperature is the factor that has a great influence on the emitting intensity of a phosphor.[12] Therefore, thermal stability is one of the important characteristics that needs to be taken into consideration before recommending the phosphor for potential applications.[15] The PL spectra of the temperature dependence experiment are shown in Fig. 11. As we can observe from Fig. 11, the luminescence intensity shows a gradual decrease when the sample was heated and the phosphor still maintains 55% of the emitting intensity at 150 °C compared with the initial intensity

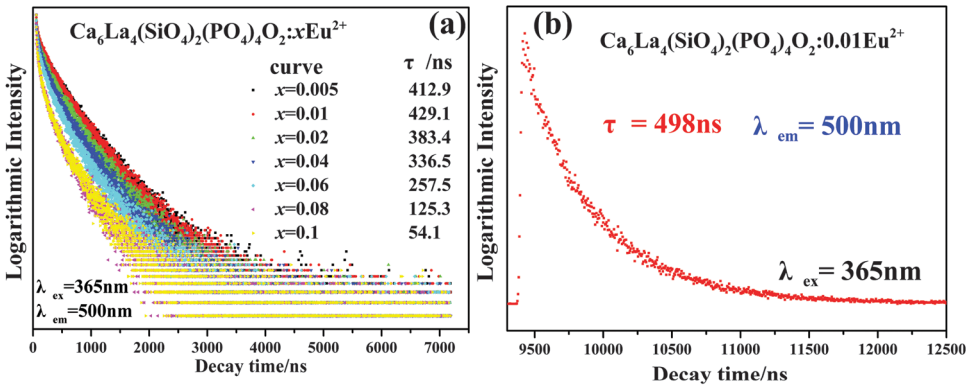

Fig. 10 (a) Room-temperature and (b) low-temperature decay curves of $Ca_6La_4(SiO_4)_2(PO_4)_4O_2$:0.01$Eu^{2+}$.

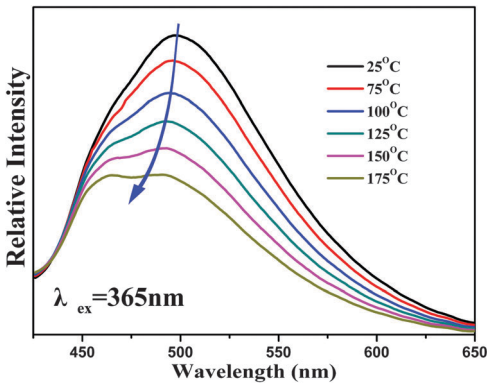

Fig. 11 Temperature-dependent spectra of $Ca_6La_4(SiO_4)_2(PO_4)_4O_2:Eu^{2+}$ ranging from 25 °C to 175 °C.

at room temperature (25 °C). Therefore, it shows better thermal stability than the garnet phosphor $Ca_2LaZr_2Ga_3O_{12}:Ce^{3+}$ and the commercial green phosphor $Ba_2SiO_4:Eu^{2+}$. On the other hand, the full width at half maximum (FWHM) of the PL spectra increases from 56 nm up to 75 nm during this temperature increase. The increase of FWHM can be explained by a configuration coordinate diagram, a physical model, that electron–phonon interaction will enhanced and the population of higher vibration levels will increase when the temperature rises,[18] and then, the excited luminescent center is thermally activated and release non-radiative through the crossover between the excited states and the ground states with the help of phonons. In consequence, the luminescence is quenched due to the enhanced population density of phonons, which also causes the broadening of the PL spectra.[4,17]

On the other hand, the PL spectra at different temperatures show a slight blue-shift, which is attributed to thermally-active phonon-assisted tunneling from the excited states of the low-energy emission band to the excited states of the high-energy emission band.[11,12] As mentioned before, there are two emission centers for the $Ca_6La_4(SiO_4)_2(PO_4)_4O_2:Eu^{2+}$ phosphor. The thermal back transfer from lower energy centers to higher energy centers will be promoted at higher temperature.[23,35] Consequently, the higher energy emission is strengthened and the blue-shift phenomenon is observed. In addition, the expanded host lattice can also cause a reduction in the crystal-field splitting and lead to a higher energy emission when the temperature increases.[4,36]

Luminescence efficiency is an important technological parameter for the application of a phosphor. The internal quantum efficiency (QE) of $Ca_6La_4(SiO_4)_2(PO_4)_4O_2$:0.01$Eu^{2+}$ was measured and calculated to be 57.73%. It is higher than that of $K_{0.5}Mg_{1.5}Al_4Si_5O_{13}:Eu^{2+}$ (48.3%)[11] and $Ca_2LaZr_2Ga_3O_{12}:Ce^{3+}$ (35.2%), but lower than the commercial green phosphor (Ba,Sr)SiO_4 (79%).[12] In general, the QE can be further optimized by improving the preparation conditions because the QE depends closely on crystalline defects, particle sizes and the morphology of the phosphor.[8,37] To demonstrate the potential application, the electroluminescent spectrum of w-LED lamp is displayed in Fig. 12. The self-made lamp was fabricated by coating $Ca_6La_4(SiO_4)_2(PO_4)_4O_2:Eu^{2+}$, $BAM:Eu^{2+}$ and $CaAlSiN_3:Eu^{2+}$ phosphors on a n-UV chip (λ_{ex} = 385 nm). The CIE color coordinates, CCT and Ra of the self-fabricated w-LED lamp were calculated to be (0.37, 0.37), 4253 K and 86, respectively. The relatively high Ra value (86) and appropriate CCT value (4253 K) demonstrate that the $Ca_6La_4(SiO_4)_2(PO_4)_4O_2:Eu^{2+}$ can be a promising candidate for a green-emitting phosphor for the application of w-LEDs.

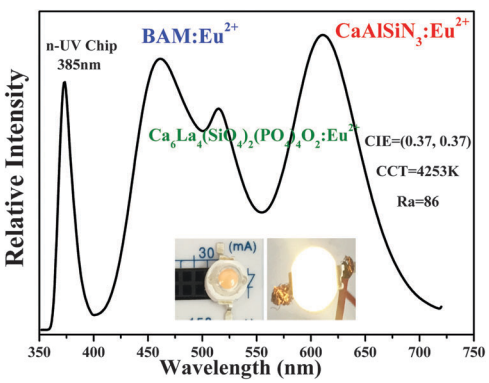

Fig. 12 EL spectrum of a white-emitting n-UV chip (385 nm) comprising $Ca_6La_4(SiO_4)_2(PO_4)_4O_2:Eu^{2+}$, $BAM:Eu^{2+}$ and $CaAlSiN_3:Eu^{2+}$ phosphors driven by 30 mA current. Inset: digital images of the LED package with and without powder input.

4. Conclusion

A novel apatite structure green phosphor $Ca_6La_4(SiO_4)_2(PO_4)_4O_2:Eu^{2+}$ has been synthesized by a high-temperature solid-state reaction method. The phase purity and elemental valency were examined according XRD and XPS. The crystal structure information was refined by Rietveld refinement using the high quality XRD traces. The refinement parameters, all atom positions and occupancy factors for $Ca_6La_4(SiO_4)_2(PO_4)_4O_2:0.01Eu^{2+}$ were presented and the coordination environments of the two types of cation sites were discussed in detail. In the section on luminescence properties analysis, the asymmetric emission spectrum, which is attributed to the electric dipole-allowed transition of the Eu^{2+} ions from excited 5d state to the 4f ground state, was resolved into two Gaussian components peaking at 492 nm and 593 nm, demonstrating the existence of two emitting centers. Moreover, this result was further proved by low-temperature luminescence experiments. Based on the coordination environments analysis and an empirical relation proposed by Van Uitert, we propose that the higher energy emission band (492 nm) will be detected when Eu^{2+} is located at the 4h site and the lower energy emission band (539 nm) is derived from the Eu^{2+} ion occupying the 6h site. The optimized Eu^{2+} concentration was confirmed to be x = 0.01, the R_c is calculated to be 20.09 Å and the energy transfer between Eu^{2+} is of the exchange interaction type. The phosphor shows good thermal stability, it maintain 55% of its emitting intensity at 150 °C compared with room temperature. Finally, the $Ca_6La_4(SiO_4)_2(PO_4)_4O_2:Eu^{2+}$ phosphor was fabricated with commercial red ($CaAlSiN_3:Eu^{2+}$) and blue (BAM:Eu^{2+}) phosphors on a n-UV chip excited at 385 nm; the CIE color coordinates, CCT and Ra of the self-fabricated w-LED lamp were calculated to be (0.37, 0.37), 4253 K and 86, respectively. This proves that this green phosphor has the potential to be used in a w-LED lamp.

Acknowledgements

This study was sponsored by the National Natural Science Foundation of China (Grant No. 51472223), the Program for New Century Excellent Talents in University of Ministry of Education of China (Grant No. NCET-12-0951) and the Fundamental Research Funds for the Central Universities (Grant No. 2652015020 and Grant No. 2652015008).

References

1 C. H. Huang, Y. C. Chiu, Y. T. Yeh, T. S. Chan and T. M. Chen, *ACS Appl. Mater. Interfaces*, 2012, **4**, 6661–6668.
2 S. Ye, F. Xiao, Y. X. Pan, Y. Y. Ma and Q. Y. Zhang, *Mater. Sci. Eng., R*, 2010, **71**, 1–34.
3 W. Wang, W. Yang, Z. Liu, H. Wang, L. Wen and G. Li, *Sci. Rep.*, 2015, **5**, 11480.
4 W. Xiao, X. Zhang, Z. Hao, G.-H. Pan, Y. Luo, L. Zhang and J. Zhang, *Inorg. Chem.*, 2015, **54**, 3189–3195.
5 W. Wang, *J. Mater. Chem. C*, 2014, **2**, 9342–9358.
6 G. Li, W. Wang, W. Yang and H. Wang, *Surf. Sci. Rep.*, 2015, **70**, 380–423.
7 M. Shang, C. Li and J. Lin, *Chem. Soc. Rev.*, 2014, **43**, 1372–1386.
8 J. Chen, Y. Liu, M. Fang and Z. Huang, *Inorg. Chem.*, 2014, **53**, 11396–11403.
9 W. Wang, H. Yang and G. Li, *J. Mater. Chem. C*, 2013, **1**, 4070–4077.
10 W. Wang, Y. Lin, W. Yang, Z. Liu, S. Zhiou, H. Qian, F. Gao, L. Wen and G. Li, *J. Mater. Chem. C*, 2014, **2**, 4112–4116.
11 J. Zhou, Z. Xia, M. Chen, M. S. Molokeev and Q. Liu, *Sci. Rep.*, 2015, **5**, 12149.
12 J. Zhong, W. Zhuang, X. Xing, R. Liu, Y. Li, Y. Liu and Y. Hu, *J. Mater. Chem. C*, 2015, **119**, 5562–5569.
13 X. Wang and Y. Wang, *J. Mater. Chem. C*, 2015, **119**, 16208–16214.
14 H. Liu, Y. Luo, Z. Mao, L. Liao and Z. Xia, *J. Mater. Chem. C*, 2014, **2**, 1619.
15 Z. Xia, M. S. Molokeev, W. B. Im, S. Unithrattil and Q. Liu, *J. Mater. Chem. C*, 2015, **119**, 9488–9495.
16 G. Li, D. Geng, M. Shang, Y. Zhang, C. Peng, Z. Cheng and J. Lin, *J. Mater. Chem. C*, 2011, **115**, 21882–21892.
17 J. Chen, Y.-g. Liu, L. Mei, Z. Wang, M. Fang and Z. Huang, *J. Mater. Chem. C*, 2015, **3**, 5516–5523.
18 J. Chen, Y. Liu, L. Mei, H. Liu, M. Fang and Z. Huang, *Sci. Rep.*, 2015, **5**, 9673.
19 S. Schmiechen, P. Strobel, C. Hecht, T. Reith, M. Siegert, P. J. Schmidt, P. Huppertz, D. Wiechert and W. Schnick, *Chem. Mater.*, 2015, **27**, 1780–1785.
20 H. Ji, Z. Huang, Z. Xia, M. S. Molokeev, X. Jiang, Z. Lin and V. V. Atuchin, *Dalton Trans.*, 2015, **44**, 7679–7686.
21 N. Guo, H. You, C. Jia, R. Ouyang and D. Wu, *Dalton Trans.*, 2014, **43**, 12373–12379.
22 S. Miao, Z. Xia, J. Zhang and Q. Liu, *Inorg. Chem.*, 2014, **53**, 10386–10393.
23 W. B. Dai, Y. F. Lei, T. Yu, M. Y. Peng and Q. Y. Zhang, *Mater. Res. Bull.*, 2015, **67**, 176–184.
24 W. Lv, M. Jiao, Q. Zhao, B. Shao, W. Lu and H. You, *Inorg. Chem.*, 2014, **53**, 11007–11014.
25 M. Peng, X. Yin, P. A. Tanner, M. G. Brik and P. Li, *Chem. Mater.*, 2015, **27**, 2938–2945.
26 Y. Zhang, G. Li, D. Geng, M. Shang, C. Peng and J. Lin, *Inorg. Chem.*, 2012, **51**, 11655–11664.
27 K. Fengwen, Z. Yi and P. Mingying, *Inorg. Chem.*, 2015, **54**, 1462–1473.
28 H. Lin, J. Xu, Q. Huang, B. Wang, H. Chen, Z. Lin and Y. Wang, *ACS Appl. Mater. Interfaces*, 2015, **7**, 21835–21843.
29 K. A. Denault, J. Brgoch, M. W. Gaultois, A. Mikhailovsky, R. Petry, H. Winkler, S. P. DenBaars and R. Seshadri, *Chem. Mater.*, 2014, **26**, 2275–2282.
30 C.-H. Huang, P.-J. Wu, J.-F. Lee and T.-M. Chen, *J. Mater. Chem.*, 2011, **21**, 10489.
31 R. Yu, J. Wang, Z. Zhao, M. Li, S. Huo, J. Li and J. Wang, *Mater. Lett.*, 2015, **160**, 294–297.

32 Z. Wang, Z. Xia, M. S. Molokeev, V. V. Atuchin and Q. Liu, *Dalton Trans.*, 2014, **43**, 16800–16804.
33 R. Yu, N. Xue, J. Li, J. Wang, N. Xie, H. M. Noh and J. H. Jeong, *Mater. Lett.*, 2015, **160**, 5–8.
34 J. Chen, Y.-g. Liu, H. Liu, D. Yang, H. Ding, M. Fang and Z. Huang, *RSC Adv.*, 2014, **4**, 18234.
35 X. Zhang, J. Wang, L. Huang, F. Pan, Y. Chen, B. Lei, M. Peng and M. Wu, *ACS Appl. Mater. Interfaces*, 2015, **7**, 10044–10054.
36 C. Zhao, Z. Xia and S. Yu, *J. Mater. Chem. C*, 2014, **2**, 6032.
37 S. Miao, Z. Xia, M. S. Molokeev, M. Chen, J. Zhang and Q. Liu, *J. Mater. Chem. C*, 2015, **3**, 4616–4622.